Chapter 8

Pre-galactic enrichment of the IGM

8.1 Summary

We examine the dynamical evolution and statistical properties of the supernova ejecta of massive primordial stars in a cosmological framework to determine whether this first population of stars could have enriched the universe to the levels and dispersions seen by the most recent observations of the Lyman-α forest. We evolve a ΛCDM model in a 1 Mpc^3 volume to a redshift of $z = 15$ and add "bubbles" of metal corresponding to the supernova ejecta of the first generation of massive stars in all dark matter halos with masses greater than $5 \times 10^5 M_\odot$. These initial conditions are then evolved to $z = 3$ and the distribution and levels of metals are compared to observations. In the absence of further star formation the primordial metal is initially contained in halos and filaments. Photoevaporation of metal-enriched gas due to the metagalactic ultraviolet background radiation at the epoch of reionization ($z \sim 6$) causes a sharp increase of the metal volume filling factor. At $z = 3$, $\sim 2.5\%$ of the simulation volume ($\approx 20\%$ of the total gas mass) is filled with gas enriched above a metallicity of $10^{-4} Z_\odot$, and less than 0.6% of the volume is enriched above a metallicity of $10^{-3} Z_\odot$. This suggests that, even with the most optimistic prescription for placement of primordial supernova and the amount of metals produced by each supernova, this population of stars cannot entirely be responsible for the enrichment of the Lyman-α forest to the levels and dispersions seen by current observations unless we have severely underestimated the duration of the Pop III epoch. However, comparison to observations using carbon as a tracer of metals shows that Pop III supernovae can be significant contributors to the very low overdensity Lyman-α forest. This chapter has been previously published as a paper in the Astrophysical Journal [1].

8.2 Motivation

Recent observations by Schaye et al. and Aguirre et al. [84, 85] have shown that the Lyman-α forest is polluted with metals at very low densities. The distribution of metal is very strongly dependent on overdensity, with median metallicity values ranging from $[C/H] = -4.0$ at $\log \delta = -0.5$ (where δ is defined as ($\delta \equiv \rho/\bar{\rho}$) to $[C/H] = -2.5$ at $\log \delta = 2.0$ using their fiducial UV background model. Their observations show little evidence for metallicity evolution of the Lyman-α forest over the redshift range $z = 1.5 - 4.5$.

The lack of observed evolution in metallicity is suggestive of a very early epoch of stellar evolution. Recent observations by the Wilkinson Microwave Anisotropy Probe suggest an epoch of star formation in the redshift range of $z = 11 - 30$ [64], which is consistent with the simulation results of Abel et al. [39] and Bromm et al.[42], which suggest that the first generation of stars (known as Population III, or Pop III) formed in the redshift range $z = 20 - 30$. The Abel et al. results, which are the highest-resolution simulations of formation of the first generation of primordial stars to date, also suggest that Pop III stars are very massive - on the order of $\sim 200 M_{\odot}$. Stars that are in this mass range will die in extremely energetic pair-instability supernovae and can eject up to 57 $M_{\odot}$ of ^{56}Ni [60, 61]. The formation site of Pop III stars is in halos with total masses of $\sim 10^6 M_{\odot}$. [39, 228]. These halos have escape velocities which are on the order of a few km/s. Due to the shallowness of the potential wells that Pop III stars form in, Ferrara [229] suggests that ejecta from a massive Pop III supernova can propagate to very large distances (far greater than the halo virial radius), a result which is supported in simulations performed by Bromm et al.[95].

In this chapter we describe the results of cosmological hydrodynamic simulations which address whether or not a population of massive primordial stars can be responsible for metal enrichment of the Lyman-α forest to the level and dispersion seen today. We examine the most optimistic possible scenario for Pop III star formation and enrichment in order to establish an upper limit on metal enrichment of the Lyman-α forest due to Population III stars.

8.3 Problem Setup

The simulations were set up using the concordance cosmological model ($\Omega_m = 0.3$,$\Omega_\Lambda = 0.7$, $\Omega_b = 0.04$ and a Hubble parameter of $h = 0.7$ where h is in units of 100 km s^{-1} Mpc^{-1}. Initial perturbations in the dark matter and baryon density were created with an Eisenstein & Hu [194] power spectrum with $\sigma_8 = 0.9$ and $n = 1$ using the Zel'dovich approximation [125] in a box which is 0.7 h^{-1} comoving Mpc on a side. In our simulations we use a computational box with 256^3 grid cells with a comoving spatial resolution of $2.7h^{-1}$ kpc and a dark matter mass resolution of 1477 h^{-1} $M_{\odot}$.

The simulation was initialized at z=99 and was allowed to evolve to z=15 using the Eulerian adaptive mesh refinement code Enzo (as described in Chapter 2). The simulation was stopped at $z = 15$ and all halos with dark matter mass $M_{DM} \geq 5 \times 10^5$ $M_\odot$ were found using the HOP halo-finding algorithm [196]. This yielded 184 halos, each of which we assume produces one pair instability supernova. Note that we are ignoring negative feedback, which raises the minimum halo mass which can form Pop III stars [**?**]. This is consistent with our desire to simulate a best-case scenario. We discuss this and other assumptions in Section 8.5.

At this point, two separate cases are considered. In the first case (referred to as Case 'A'), spheres of uniform metal density 1 kpc (proper) in radius with 127 $M_\odot$ of metal are placed in the simulation, centered on the cell of highest dark matter density of each halo. This corresponds to a mass averaged metallicity in the volume of $< Z > \equiv M_Z/M_B = 4.02 \times 10^{-5}$ $Z_\odot$ (where M_Z and M_B are total metal and baryon masses in the simulation volume), which remains constant throughout the simulation. No other modifications to the data were made – in particular, the baryon density, temperature and peculiar velocities and dark matter density were unmodified.

In the second case (Case 'B'), the spheres of uniform metal density are placed down in the same manner. In addition, the baryon gas in the corresponding volume is smoothed to the cosmic mean ($< \rho >= \Omega_b \rho_c$), and the temperature of the baryon gas is set to 10^4 K. This corresponds to the net smoothing and heating of baryons in primordial halos due to pair-instability supernovae. The mass averaged metallicity in this case is slightly greater, $< Z >= 4.11 \times 10^{-4}$ $Z_\odot$. This is due to a small net loss in baryon mass when the densities are smoothed. As in Case A, peculiar velocities and dark matter density are unmodified.

The simulations are then evolved to z=3, following the evolution of the gas using non-equilibrium chemistry and cooling from hydrogen and helium and their ions [152, 153]. Metal line cooling is ignored. At z = 7 we initialize a uniform metagalactic ultraviolet background field [230] with a slope of $q_\alpha = -1.8$ that is ramped to a pre-computed value by a redshift of z = 6. Zhang et al. [231] determined that such a prescription can reproduce the Gunn-Peterson effect in the hydrogen Ly-α lines by a redshift of 5.5. Self-shielding of the gas is not explicitly included in the assumed UV background.

It is important to note that the box size, at 0.7 h^{-1} Mpc, is somewhat small. Statistical results are reliable at $z = 15$. However, by $z = 3$ (when the simulations are terminated) the box is too small to be statistically reliable. We also performed a simulation in eight times the volume at the same mass and spatial resolution (i.e. 512^3 cells/particles), which gave results indistinguishable from what follows. Nonetheless, all results at late times should be considered qualitative.

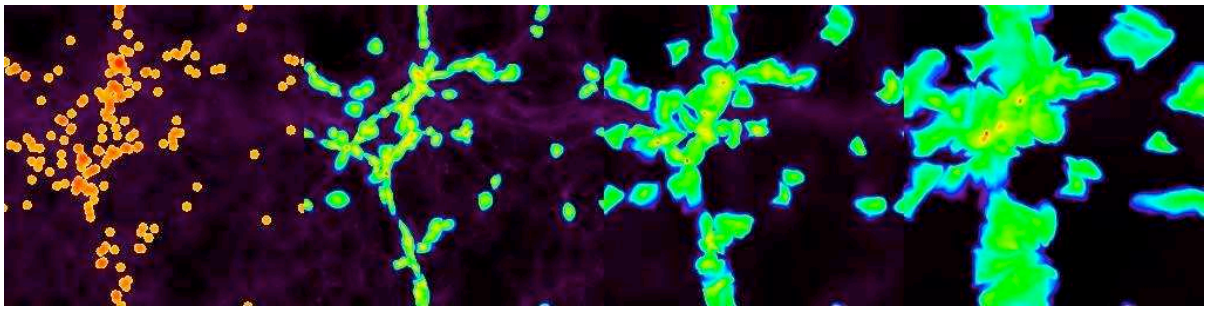

Figure 8.1: Projected log metal density (Case A). The area viewed is a projection of the entire simulation volume. The four panels correspond to (from left to right) z=15, 7, 5 and 3. The Pop III supernova remnants are placed in the volume at z=15 and advect along the filaments. Photoevaporation of gas in the filaments, driven by the metagalactic UV background, causes the volume filling factor of the metal-enriched gas to increase substantially by z=3.

8.4 Results

The general evolution of our simulation after injection of metal bubbles at $z = 15$ is as follows: Beginning at $z = 15$, the bubbles of metal track the flow of gas onto and along dark matter filaments. The competing effects of advection along the filaments and the collapse of filaments during this period essentially cancel out, with little net effect on the fraction of the volume occupied by metal enriched gas (also referred to as the volume filling factor, or VFF). Regions of relatively high metallicity ($Z \geq 10^{-3} Z_{\odot}$), corresponding to the densest regions of filaments, decrease their volume filling factor significantly from z=15 to z=6. Case A shows more of a decrease in VFF at relatively high metallicities (from a VFF of $10^{-2.5}$ to $10^{-3.2}$) than Case B does (which has a minimum VFF of $10^{-2.9}$) due to the higher initial densities and lower initial temperatures of polluted regions in Case A. Figure 8.1 shows snapshots of the metal distribution in the simulation volume taken at 4 different redshifts, and Figure 8.2 shows the volume filling factor for three metallicity thresholds as a function of redshift.

A uniform metagalactic ultraviolet background is switched on at $z = 7$. Photoheating raises the mean temperature of the baryon gas. In the Lyman-α forest overdensity regime ($1 \leq \delta \leq 10$), which roughly corresponds to the filamentary structure observed in Figure 8.1, the temperature is raised to $\sim$ 10,000 K. The local thermal speed of the baryon gas then exceeds the escape velocity of the filaments, resulting in significant expansion of the volume occupied by the gas in those filaments. This includes the gas polluted by metals. This effect can be clearly seen in the third and fourth panels of Figure 8.1. Figure 8.2 shows the sharp increase in metal VFF in a more quantitative way. Gas

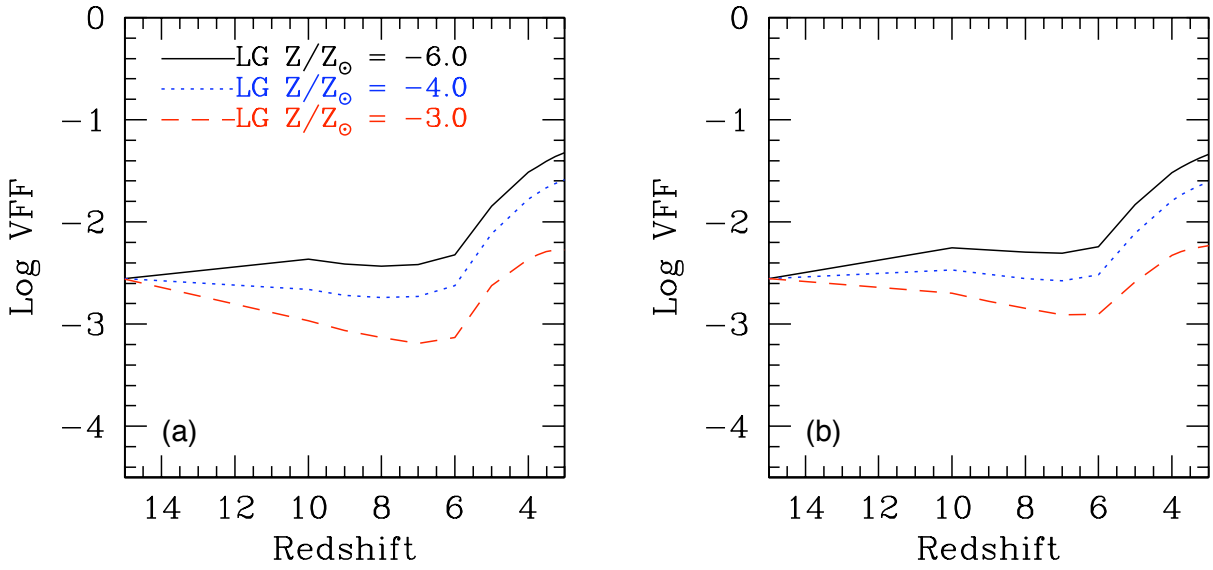

Figure 8.2: Volume filling factor. The lines describe the fraction of the simulation volume filled to a metallicity of at least 10^{-6} $Z_\odot$ (black), 10^{-4} $Z_\odot$ (blue) and 10^{-3} $Z_\odot$ (red). Panel (a) corresponds to the simulation where spheres of uniform metal density are added and no other changes are made. Panel (b) corresponds to the simulation where, in addition to uniform spheres of metal density, the baryon density in the corresponding volume is smoothed to the mean density of the simulation and the gas temperature of the sphere is raised to 10^4 K.

which has been polluted above a metallicity of $10^{-6}Z_{\odot}$ (corresponding to essentially the entire volume of gas polluted by metals) increases in VFF to 0.048 for both Case A and 0.046 for Case B. This corresponds to 28% (26%) of the baryon mass being enriched for Case A (Case B). The two cases are essentially indistinguishable with regards to the total mass and volume of gas polluted by metals. Examination of gas with higher metallicity ($Z \geq 10^{-3}Z_{\odot}$) shows some difference between the cases, with a maximum VFF of 5.2×10^{-3} for Case A and 5.8×10^{-3} for Case B (corresponding to 1.5% and 1.9% of the total gas mass, respectively). This difference is due to the initial smoothing and heating of baryons in Case B.

In Figure 8.3 we estimate the amount of carbon contained within the primordial metallicity field at $z = 3$. We assume that the carbon abundance in the metal density is equal to $X_C = 0.027$, which is taken from the supernovae metal yield of a massive primordial star of approximately 260 $M_{\odot}$ as computed by Heger et al. [**?**]. We then compute the mean and median carbon metallicity, $[C/H] = \log(n_C/n_H) - [C/H]_{\odot}$ (where $[C/H]_{\odot} = -3.45$) in bins of constant logarithmic overdensity between $\log \delta = -0.5 - 2.0$ and plot this in Panel A of Figure 8.3. Altering the effects of X_C results in this figure being scaled along the y-axis by a factor of $\log(X_C/0.027)$. The solid green line is the fit to the observations of Schaye et al. [84] using their fiducial model. The dashed-green line is the fit of the lower bound lognormal scatter of their data. The results of our simulation yield that the Population III carbon content in the IGM at $z = 3$ is below the observed limits across the entire overdensity range.

In Panel B of Figure 8.3 we plot the probability distribution function (PDF) for both simulation cases in the overdensity range $\log \delta = -0.5$ to $+2.0$. The vertical lines correspond to the mean (solid) and median (dashed) values of the [C/H] values. The distributions corresponding to the two cases are statistically indistinguishable within one standard deviation. The small variation between the two cases in the range [C/H]=-4 to -2 is due to the difference in their mean initial metallicity per bubble (caused by the difference in treatment of of the baryon density field in the region initially polluted by metals in the two cases).

In order to determine the observability of the primordial metallicity field, we post-process our data to compute the fraction of CIV to neutral hydrogen (HI) for each cell in our computational volume. Obtaining the quantity $log\ F = log\ (n_{CIV}/n_{HI})$ within constant overdensity bins, in the range $log\ \delta = -0.5 - 2.0$, allows the determination of the lognormal average $< log\ F >$ at each redshift. At z=3 our analysis yields $< log\ F >= -3.78 \pm 0.91 (-3.78 \pm 0.92)$ for Case A (B). We can then approximate the CIV optical depth due to Pop III stars as $\tau_{CIV}^{popIII} \approx (\frac{f_{CIV}\lambda_{CIV}}{f_{HI}\lambda_{HI}}) \cdot 10^{<log\ F>} \tau_{HI}$, where $f_{CIV,HI}$ and $\lambda_{CIV,HI}$ are the oscillator strengths and rest-frame absorption wavelengths for the two species (CIV & HI). Using our mean values for $< log\ F >$ at z=3 we obtain an estimated optical depth, due to CIV, of $\tau_{CIV}^{popIII} = 0.97^{7.86}_{0.12} \times 10^{-4}\ \tau_{HI}$ ($0.97^{8.13}_{0.11} \times 10^{-4} \tau_{HI}$). Schaye et al. [84] computed $\tau_{CIV} = 10^{-2}\ \tau_{HI}$ in the Ly-α forest overdensity range. If

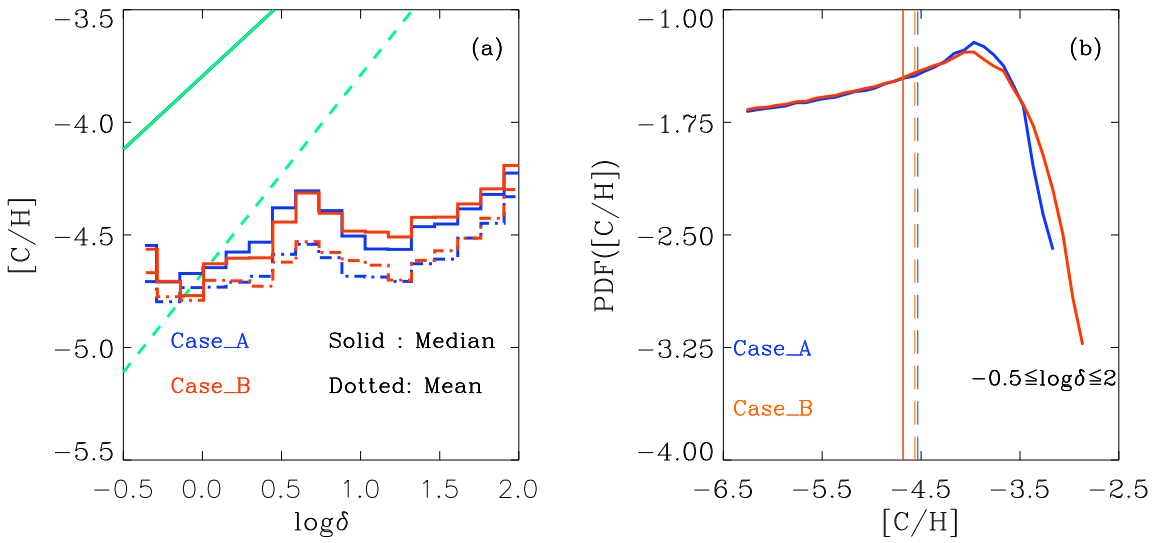

Figure 8.3: In panel (a) we plot the volume averaged $[C/H]$ in solar units within constant logarithmic overdensity bins in the range of $1 \leq \delta \leq 10^2$ at $z = 3$. The profiles for the two cases discussed in the text show no statistical difference. In panel (b) we plot the probability distribution function (PDF) of $[C/H]$ within the overdensity range $1 \leq \delta \leq 10^2$. The y-axis measures the fraction of the metal polluted volume with [C/H] values between [C/H] and [C/H]+Δ[C/H]. The result is computed with $X_C = 0.027$. The two distributions yield $< [C/H] >= -4.68 \pm 0.80$ for Case A and $< [C/H] >= -4.68 \pm 0.81$ for Case B. Median values for the two PDFs are -4.53 and -4.56 respectively. The two cases are indistinguishable within one standard deviation.

the above value corresponds to the total metallicity at z=3 then the contribution of the primordial component to the total optical depth of CIV is about $\tau_{CIV}^{popIII} = 0.01\ \tau_{CIV}$. This result is somewhat sensitive to the shape of the UV background – see Schaye et al. [84] for more details. Statistical correlations between Pop III CIV and HI absorbers and more detailed examination of spectra due to ejecta from Population III stars will be discussed in a forthcoming paper.

8.5 Discussion

In this chapter we use cosmological hydrodynamic simulations to examine the evolution of metals ejected by an early population of massive primordial stars. We show that, in the absence of further star formation, photoevaporation of baryons bound to dark matter filaments during reionization is the most important mechanism in determining the volume filling fraction by $z = 3$. Our two study cases, although different in their initial setup, give the same results for the global distribution of the primordial metal field by $z = 3$, suggesting that our result is insensitive to small-scale dynamics.

Comparison of our results to observations of carbon in the Lyman-α forest by Schaye et al. [84] show that at $z = 3$ the median value of the Pop III carbon metallicity for both cases considered fall within the low end of the scatter range of the observed data for $\log \delta \leq 0$. For $\log \delta \geq 0$ the Population III carbon metallicity is below the observed values, with the Schaye result showing a much stronger increase in metallicity with overdensity, resulting in the median value of $[C/H]^{PopIII}$ becoming an increasingly smaller fraction of the total observed [C/H].

Our results depend strongly on two factors, namely, the total number of Population III stars formed in our volume and the metal yield per star. In these simulations we make the assumption that all halos with mass $M_{DM} \geq 5 \times 10^5 M_\odot$ form a massive primordial star by $z = 15$, which was guided by the simulations performed by Abel et al. [**?**] and Yoshida et al. [228], which show that this is the characteristic dark matter mass of a halo which forms a star in the early universe. Simulations by Machacek et al. [71] and semianalytical calculations by Wise & Abel [97] show that a soft UV background produced by the first Pop III stars effectively dissociates H_2, which is the primary cooling mechanism in primordial star formation. This so-called negative feedback effect raises the minimum halo mass that can form a primordial star within it and therefore reduces the number of halos which will form Population III stars at a given epoch. Wise & Abel [97] find that negative feedback reduces the number of star forming halos by a factor of 5-10 relative to what we used. On the other hand, suppression of Pop III star formation by negative feedback would be compensated by an extended epoch of Pop III star formation. At present, we do not know when Pop III star formation ceases. We view our choice of $M_{min} = 5 \times 10^5 M_\odot$ at $z = 15$ as a hedge between competing effects.

The decision to place spheres of metal in the simulation volume at $z = 15$ was guided primarily by the WMAP polarization results [64]. This choice may have resulted in an underestimation of the number of Population III stars (and therefore metal pollution due to Pop III supernovae) because there are dark matter halos which form after $z = 15$ but may still be unpolluted by metals. However, results by Bromm et al. [93] suggest the existence of a "critical metallicity" of $\sim 5 \times 10^{-3} Z_{\odot}$ above which a solar IMF dominates, and it has been argued that this metallicity is reached by $z \sim 15 - 20$ [232, 233]. The choice of $z = 15$ for our epoch of instantaneous metal enrichment seems to be a reasonable compromise.

The physical properties of the metal "bubbles" can have a possible effect on our results. The choice of a 1 kpc (proper) radius for the metal bubbles is somewhat arbitrary. Several calculations have been performed that suggest that ejecta from the most massive pair-instability supernovae can propagate to large distances [95, 234], but the maximum propagation distance is unclear. Additionally, Bromm et al. [95] suggest that the ejecta from pair-instability supernovae still has substantial peculiar velocities ($\sim$ 50 km/s) at 500 pc. The metal spheres in this calculation have no initial outward peculiar velocity, which may result in a smaller volume filling factor than if this were taken into account.

The second factor that strongly affects our result is the choice of the amount of metals created per Population III supernova. Abel et al. [39] and Bromm et al. [42] both suggest that the first population of stars will be very massive. The mass function of the first generation of stars is unclear, due to lack of resolution and appropriate physics. The main-sequence mass of the star strongly affects its ultimate fate: Stars with the range of $\sim 140 - 260 M_{\odot}$ detonate in pair instability supernovae, which are much more energetic (up to $\sim 10^{53}$ ergs compared to 10^{51} ergs for a standard Type I or Type II supernova) and produce more metal (up to 57 $M_{\odot}$ of ^{56}Ni and almost 130 $M_{\odot}$ of total metals for a 260 $M_{\odot}$ primordial star). However, stars between $\sim 50 - 140 M_{\odot}$ and above $\sim 260 M_{\odot}$ form black holes without first ejecting significant quantities of nucleosynthesized material [61]. The amount of metals placed into the simulation volume is scalable - if the mean amount of metals ejected by Population III stars were lower (due to some substantial fraction collapsing directly into black holes, for instance), all of the results shown in Figure 8.2 and Panel A of Figure 8.3 scale linearly with the mean amount of metal produced per star.

Our results for [C/H] vs. overdensity (using carbon as a proxy for metallicity) agree with the results of Schaye et al. [84] to within one standard deviation for the lowest observed densities ($\log \delta < 0$). These are the densities that are the most likely to remain unpolluted by later generations of stars, which form in deeper potential wells. Further study of the lower density regions of the Lyman-α forest could yield more constraints on the mass and total number density of massive Population III stars.

An additional factor to consider is that the nucleosynthetic yields of very massive primordial stars are much different than that of metal-enriched stars [61]. Due to this,

it may be possible to disentangle the effects of massive primordial stars and their metal-polluted descendants, as discussed by Oh et al. [235].

Due to our choices of low minimum halo mass and high metal yield per supernova, our result is a strong upper limit on the pollution of the Lyman-α forest due to Population III stars, unless we have severely underestimated the duration of the Population III epoch.

The simulation volume is relatively small. Though a reasonable statistical representation of the universe at $z = 15$, the results obtained at later times ($z \sim 3$) should be considered qualitative due to the small box size. A much larger simulation volume is required for adequate statistics at $z \sim 3$. However, simulating a much larger volume which would still have reasonable spatial and dark matter mass resolution on a single grid is computationally prohibitive at the present time.

All of the simulation results described in this paper are performed without further star formation or feedback. Having a single episode of star formation at $z = 15$ means that metal evolution after that time is passive, whereas in reality there would be continuous star formation and feedback. A logical extension of this work is the inclusion of later epochs of star formation and their resulting feedback of metals and energy into the IGM. These results will be presented in a forthcoming paper.